Phase separation and the phase diagram of cuprate superconductors

2007 J. Phys.: Condens. Matter 19 086218

(http://iopscience.iop.org/0953-8984/19/8/086218)

IOP PUBLISHING JOURNAL OF PHYSICS: CONDENSED MATTER

J. Phys.: Condens. Matter **19** (2007) 086218 (14pp) doi:10.1088/0953-8984/19/8/086218

Phase separation and the phase diagram of cuprate superconductors

E V L de Mello and D H N Dias

Instituto de Física, Universidade Federal Fluminense, Niterói, RJ 24210-340, Brazil

E-mail: evandro@if.uff.br

Received 31 August 2006, in final form 5 January 2007
Published 9 February 2007
Online at stacks.iop.org/JPhysCM/19/086218

Abstract

We show that the main features of the cuprate superconductor phase diagram can be derived considering the disorder as a key property of these materials. Our basic point is that the high pseudogap line is an onset of phase separation which generates compounds made up of regions with distinct doping levels. We calculate how this continuous temperature dependent phase separation process occurs in high critical temperature superconductors (HTSC) using the Cahn–Hilliard approach, originally applied to study alloys. Since the level of phase separation varies for different cuprates, it is possible that different systems with average doping level p_m exhibit different degrees of charge and spin segregation. Calculations on inhomogeneous charge distributions in the form of stripes on finite clusters performed by the Bogoliubov–de Gennes superconducting approach yield good agreement between the onset of local pairing amplitude and the pseudogap temperature $T^*(p_m)$. Assuming that the local order parameters generated at these clusters have their phase locked, we can follow how the superconducting phase develops at $T_c(p_m)$ by possible percolation or Josephson coupling.

(Some figures in this article are in colour only in the electronic version)

1. Introduction

After almost 20 years of research, the high critical temperature superconductors (HTSCs) still remain an unsolved problem [1–3]. All HTSCs have a similar universal complex electronic phase diagram: the parent (undoped) compound is an antiferromagnetic Mott insulator; the superconducting phase has a dome shape at low doping and low temperature. The normal phase has a pseudogap in the underdoped region at low temperatures and a metallic phase at high temperatures in the overdoped region. Understanding the complexity of such a normal phase is believed to be essential for solving the mechanism of HTSCs [1].

Another intriguing fact is the question of the inhomogeneities in these materials; some families of compounds have a high inhomogeneous electronic structure which displays either stripe [4], patchwork [5], chequerboard [6], or other forms [7]. On the other hand, depending on the type of experiment, there are some HTSC materials that appear to be more homogeneous or, at least, do not display any gross inhomogeneity [8, 9]. It is possible that these distinct features are due to a phase separation transition that produces different degrees of local hole doping densities and, consequently, different properties. We have already discussed this possibility in a previous paper [10] and we now perform more detailed calculations in connection with several new experimental data.

Recent angle resolved photoemission (ARPES) experiments with improved energy and momentum resolution [11–14] have distinguished two electronic components in $\vec{k}$-space associated with the $La_{2-x}Sr_xCuO_4$ (LSCO) system: a metallic quasi-particle spectral weight in the $(\pi/2, \pi/2)$ nodal direction which increases with hole doping and an insulator-like spectral weight at the end of the Brillouin zone straight segments in the $(\pi, 0)$ and $(0, \pi)$ antinodal regions which are almost incentive to the doping level. Comparison with the non-superconducting $La_{2-x-y}Nd_ySr_xCuO_4$ system [12], in which static stripes were first observed [4], demonstrated that the antinodal spectral weight behaviour is compatible with a quasi-one-dimensional electronic structure where the hole rich stripes behave as one dimensional metals and the hole poor stripes as insulators. These features demonstrated that in these compounds there are two aspects of the electronic structure [11–14]. Moreover, the large shift of the ARPES spectra [11] at the Fermi energy, which is called the *leading edge shift* and is interpreted as the superconducting gap, is maximum at the antinodal region. This is an indication of the d-wave symmetry of the superconducting order parameter, which vanishes in the nodal but is maximum in the antinodal directions.

Another technique which has been refined and revealed new aspects of HTSC is scanning tunnelling microscopy (STM). It is complementary to ARPES because it probes the differential conductance or the local superconducting gap Δ directly on the surface of the compound. New STM data with great resolution have also revealed strong inhomogeneities in the form of a patchwork of (nanoscale) local spatial variations of the density of states which is related to the local superconducting gap [5, 15, 16]. More recently it was possible to distinguish two distinct behaviours: well defined coherent and ill defined incoherent peaks depending on the exactly spectra location at a $Bi_2Sr2CaCu_2O_{8+\delta}$ (Bi2212) surface [17–19]. STM experiments have also detected a regular low energy chequerboard order in the electronic structure of the Bi2212 family above the superconducting critical temperature (T_c) [21] and at low temperature [20] and in the $Na_xCa_{2-x}CuO_2Cl_2$ [6].

A third important set of experiments to describe the HTSC phase diagram is the tunnelling current [22–24]. New techniques have recently shown the existence of two energy gaps which behaved differently under an applied magnetic field [25–27]. Tunnelling experiments using superconductor–insulator–superconductor (SIS) with insulator layers with various sizes and resistivities have also shown distinct sets of energy scales and have also led to the idea that the richness of the phase diagram as a function of doping may be due to charge inhomogeneities and charge clusters of different sizes in the Cu–O planes [28, 29].

The ARPES and STM experiments are surface probes, which may suggest that the inhomogeneities may be a surface effect, but charge disorders were also detected by bulk experiments, like the stripe phase in materials similar to LSCO [4, 30] and also local variations in the charge [31]. Another bulk sensitive experiment is nuclear magnetic and quadrupole resonance (NMR and NQR) which have provided ample evidence for spatial charge inhomogeneity in the CuO_2 planes [32–34]. Similarly, Singer *et al* [33] measured a distribution of T_1 over the Cu NQR spectrum in bulk LSCO, which can be attributed to a distribution of

holes p with a half width of $\Delta p/p \approx 0.5$. More recently, NMR results on $La_{1.8-x}Eu_{0.2}SrCuO_4$ were interpreted as evidence for a spatially inhomogeneous charge distribution in a system where the spin fluctuations are suppressed [35]. This new result is a strong indication that the charge disorder may be due to a phase separation transition.

These unusual features of cuprates led to theoretical proposals that phase separation is essential to understand their physics [36, 37]. In fact, phase segregation has been observed in $La_2CuO_{4+\delta}$ by x-ray and transport measurements [38, 39]. They have measured a spinodal phase segregation into an oxygen-rich (or hole-rich) metallic phase and an oxygen-poor antiferromagnetic phase above $T = 220$ K. Below this temperature the mobility of the interstitial oxygen becomes too low for a further segregation. $La_2CuO_{4+\delta}$ is the only system where ion diffusion has been firmly established, although there is evidence of ion diffusion at room temperature in micro-crystals of the Bi2212 superconductors at a very slow rate [40].

On the other hand, recent NMR studies on $YBa_2Cu_3O_{6+y}$ (YBCO) have demonstrated a complete absence of static phase separation or at least an absence of gross inhomogeneities [8, 9]. In contrast to what was measured in Bi2212 and in LSCO, the maximum hole doping variation Δp found in YBCO was very small [8]. Loram *et al* [9] also analysed the specific heat of YBCO and Bi2212 and concluded that there is evidence for a uniform doping density in these materials.

In this paper we develop the idea of two distinct [41] pseudogaps in which the lower one is associated with the onset of superconductivity [42]. We then take the upper pseudogap line as a line of phase separation transition, and introduce a model to make quantitative predictions through the Cahn–Hilliard (CH) approach [10, 43–45] in section 2. In this way, gross and weak disordered systems differ only by the degree of mobility or diffusion of the particles and different systems can belong to the same universality class. In section 3 we use the Bogoliubov–de Gennes (BdG) local method for the superconducting problem to calculate the local pairing amplitude in mesoscopic clusters with random, stripes, chequerboard, Gaussian and other forms of inhomogeneities of the charge density. The results on stripe-like formations applied to the LSCO system reveal a pseudogap phase characterized by the building up of superconducting islands or puddles with, as in BCS theory, their phase locked. Consequently, the superconducting phase is reached at low temperatures by the possible percolation or Josephson coupling of these islands [46–48]. The details of these calculations are discussed in section 2 and 3 with their consequences for HTSC in section 4.

2. The CH approach

Our main assumption is that the high pseudogap line, which we call $T_{ps}(p_m)$, which falls to zero near $p_m \approx 0.20$, and which is independent of the superconducting phase [3, 49], is the onset of the phase separation. Timusk and Sttat called this line a crossover boundary [2] and, due to their temperatures, it is clearly distinct from the lower pseudogap [42]. Thus, within this assumption, a given compound starts to phase separate at $T_{ps}(p_m)$ and this process increases continuously as the temperature goes down.

Therefore the phase separation in HTSC is a dynamical problem and depends strongly on the initial conditions, on the temperature and how the system is quenched below the phase separation line, the mobility of holes and ions, and so on. However, the information on most of these processes is not available and one has to work out the phase separation process backwards, that is, to use parameters which yield the final configurations of stripe, chequerboard, or other patterns. An appropriate framework to study such a process mathematically is by the CH theory [43], which we have already applied to the cuprates [10].

The CH approach to phase separation was conceived to describe the continuous transition of binary alloys, but, in principle, can be applied to any system that undergoes this type of continuous transition [43]. As we can infer from the stripe phases, in a compound with an average $p_m = 1/8$ hole per copper atom, the antiferromagnetic insulating phase has stripes of nearly zero holes per copper atom alternating with the metallic ones with larger values of the local charge density. As we discuss below, this behaviour can be well described by the CH theory.

Starting with small fluctuations of the local charge density, the CH non-linear differential equation which describes the process of phase separation with the time t at a temperature T below the phase separation transition temperature T_{ps} can be written as [10, 43]

$$\frac{\partial u}{\partial t} = -M\nabla^2(\varepsilon^2\nabla^2 u + A^2(T)u - B^2u^3), \tag{1}$$

where u is the order parameter associated with the local variation $p(\vec{x})$ in the average number of holes per copper atom p_m at a given point $\vec{x}$, defined as $u(\vec{x}) \equiv p(\vec{x}) - p_m$, and we expected $u(\vec{x}) \approx 0$ above and near T_{ps}. ε and B are fixed parameters, the parameter $A(T)$ depends on the temperature T and B and the ratio $\pm A(T)/B$ yields the two equilibrium densities. M is the mobility of the particles and dictates the timescale of the phase separation process. Compounds with larger values of M phase separate easier than those with smaller values, and, therefore, it will differentiate among the different HTSC families. As the temperature goes down below $T_{ps}(p_m)$, the two equilibrium values of the order parameter (or equilibrium densities) spread apart from one another and the energy barrier between the two equilibrium phases $E_g(T, p_m)$ also increases. $E_g = A^4(T)/B$ is proportional to $(T_{ps} - T)^2$ and here we introduce the completely new idea that E_g, which starts at $T_{ps}(p_m)$, can be identified with the upper pseudogap signal [10, 45], in agreement with several different experiments [3, 42]. A discussion of the details of the convergence criteria, boundary conditions and dependence on the initial parameters in one, two or three dimensions can be found in our previous work [44]. However, for completeness, we noticed that values of $A(T)/B \approx 1$ yield phase separation with granular patterns, and smaller values of this ratio yield stripe-like patterns [44]. Since, as we have already mentioned, stripe-like patterns were discovered in LSCO and related systems, in order to study the properties of these cuprates we performed our calculations with $A(T)/B = 1/5$ and $1/8$ in the low temperature range (below $T^*(p_m)$).

In figures 1 and 2 we display the mapping of the density order parameter for a system with $p_m = 1/8$ and with a maximum $\Delta p = 1/8$. Both figures have a small initial density fluctuation of $\Delta p = 0.02$ around p_m at $t = 0$, but figure 1 has a more random initial condition than the more symmetric case of figure 2. We notice that for larger times they are almost indistinguishable, but for shorter times they are very different. It is interesting that, despite the large time evolution, the system keeps very symmetric patterns. In figure 2(a) we can see a mixture of chequerboard and stripe formations which tend to evolve into a pure stripe phase (figure 2(b)). As the phase separation process continues, the systems evolve to a complete phase separation and the early time symmetric patterns are lost. This degree of charge phase separation can be reached very fast if the holes have large mobility M. This finding enables us to speculate that the measured differences among the HTSC families are due to different values of M. By the same token, the differences found in compounds of a given family can be attributed to differences in the quenched process, that is, the rate of cooling below $T_{ps}(p_m)$.

Another possible way to follow the whole phase separation process is to analyse the charge histogram evolution with time. Thus, in figure 3 we show the phase separation progress in terms of the histograms of the density order parameter. One can see the tendency, as the time flows, to evolve into a bimodal distribution around the two equilibrium conditions $p(i)_\pm = \pm A/B$.

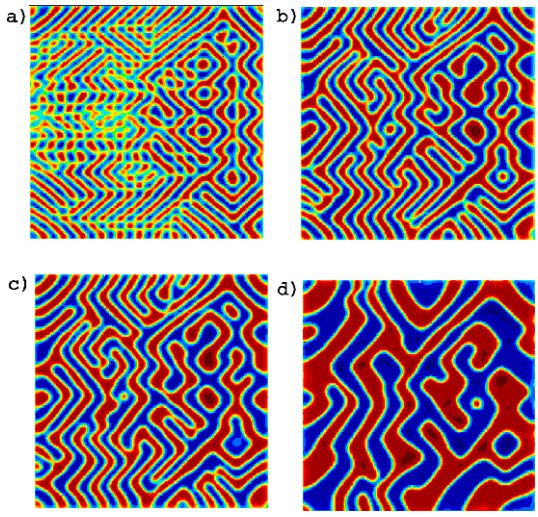

Figure 1. The mapping of the density order parameter during the process of phase separation. The initial ($t = 0$) order parameter is given by small random variations around $u = 0$. The order of the figures is (a) $t = 400$ time steps, (b) $t = 800$, (c) $t = 1000$ and (d) $t = 4000$.

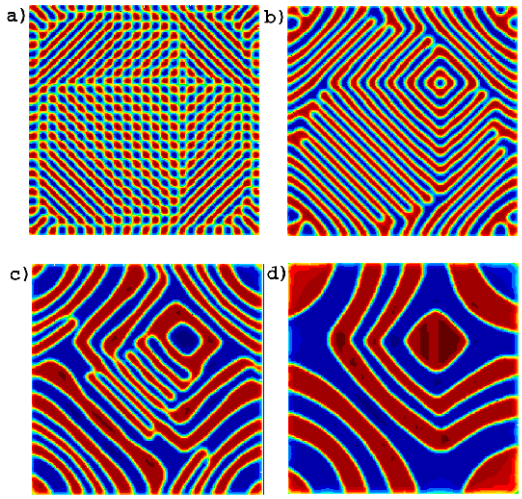

Figure 2. The same time evolution as figure 1 but with a more symmetric initial condition around $u = 0$. The order of the figures is (a) $t = 400$ time steps, (b) $t = 1000$, (c) $t = 4000$ and (d) $t = 20\,000$. For shorter times, the phase separation process develops symmetry patterns which are lost for larger times.

Thus, systems with a high mobility will probably reach a state where there are two types of regions with high and low densities. This resembles the stripe phase in the LSCO system.

Therefore, taking the large pseudogap line [3, 10, 49] as the phase separation temperature T_{ps}, it is possible to infer that the different HTSCs unfold in different patterns as described by figures 1 and 2. As a consequence, since underdoped compounds have a very high T_{ps}, they

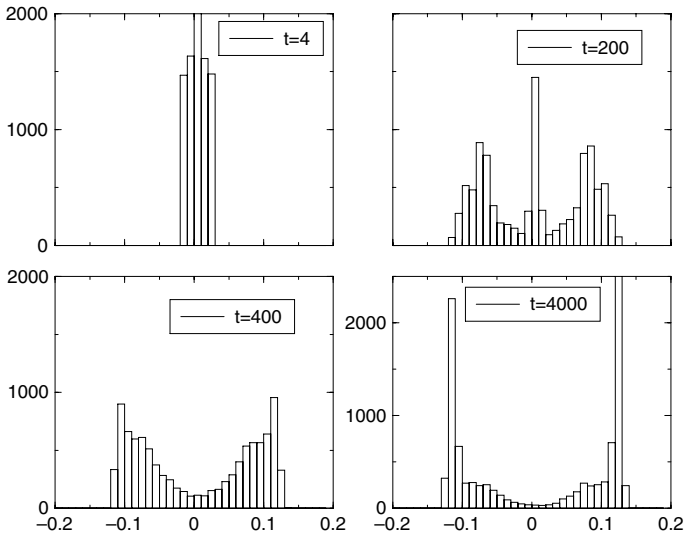

Figure 3. The time evolution histogram of the density order parameter of figure 1 with a symmetric initial condition around $u = 0$.

phase separate into a bimodal distribution faster than the optimally and overdoped compounds. The NQR results of Singer *et al* [33] suggest a bimodal distribution of charge in the LSCO system.

Thus, in order to calculate the local critical temperature for such an inhomogeneous system, we need to use the Bogoliubov–de Gennes theory. This will be outlined in the next section.

3. The local superconducting calculations

Here we discuss the main points of a local superconducting calculation to deal with the effect of the charge disorder which follows directly from the CH patterns described above. The general way to perform this, in a system without spatial invariance, is through the BdG mean-field theory, which has been largely used in the HTSC problem [50–53]. The important and novel point introduced here is that we take the initial charge distribution derived from the CH results. The procedure starts with the extend Hubbard Hamiltonian

$$H = -\sum_{\langle\langle ij\rangle\rangle\sigma} t_{ij} c^{\dagger}_{i\sigma} c_{j\sigma} + \sum_{i\sigma} (\mu_i) n_{i\sigma} + U \sum_{i} n_{i\uparrow} n_{i\downarrow} + \frac{V}{2} \sum_{\langle ij\rangle\sigma\sigma'} n_{i\sigma} n_{j\sigma'} \tag{2}$$

where $c^{\dagger}_{i\sigma}(c_{i\sigma})$ is the usual fermionic creation (annihilation) operator at site $\mathbf{x}_i$, spin $\sigma\{\uparrow\downarrow\}$, and $n_{i\sigma} = c^{\dagger}_{i\sigma} c_{i\sigma}$. t_{ij} is the hopping between sites i and j. Here we have implemented in our calculations hopping values up to fifth neighbours derived from the ARPES data for YBCO [54]. In their notation, the hopping parameters are $t \equiv t_1 = 0.225$ eV, $t_2/t_1 = -0.70$, $t_3/t_1 = 0.25$, $t_4/t_1 = 0.08$, $t_5/t_1 = -0.08$. $U = 1.1t$ is the on-site and $V = -0.6t$ is the nearest neighbour phenomenological interaction. μ_i is the local chemical potential. All the calculations presented here use the same set of parameters, and clusters with periodic boundary conditions.

$$\begin{pmatrix} K & \Delta \\ \Delta^* & -K^* \end{pmatrix} \begin{pmatrix} u_n(\mathbf{x_i}) \\ v_n(\mathbf{x_i}) \end{pmatrix} = E_n \begin{pmatrix} u_n(\mathbf{x_i}) \\ v_n(\mathbf{x_i}) \end{pmatrix}. \tag{3}$$

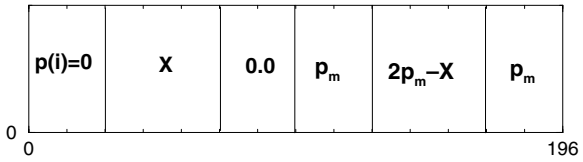

Figure 4. The low temperature stripe profile of a 14 × 14 cluster with 196 sites used to model a compound of average doping level of $p_{\rm m}$. The BdG superconducting calculations are made on these clusters and $0 \leqslant X \leqslant 0.06$ measure deviations from a bimodal charge distribution.

These BdG equations are solved self-consistently for $E_n \geqslant 0$ together with the pairing amplitude [50]

$$\Delta_U(\mathbf{x}_i) = -U \sum_n u_n(\mathbf{x}_i) v_n^*(\mathbf{x}_i) \tanh \frac{E_n}{2k_{\rm B}T}, \tag{4}$$

$$\Delta_\delta(\mathbf{x}_i) = -\frac{V}{2} \sum_n [u_n(\mathbf{x}_i) v_n^*(\mathbf{x}_i + \boldsymbol{\delta}) + v_n^*(\mathbf{x}_i) u_n(\mathbf{x}_i + \boldsymbol{\delta})] \tanh \frac{E_n}{2k_{\rm B}T}, \tag{5}$$

and the hole density is given by

$$p(\mathbf{x}_i) = 1 - 2 \sum_n [|u_n(\mathbf{x}_i)|^2 f_n + |v_n(\mathbf{x}_i)|^2 (1 - f_n)], \tag{6}$$

where f_n is the Fermi function.

We have performed self-consistent calculations with equations (5) and (6) on clusters up to 24 × 24 sites with homogeneous and inhomogeneous local doping. The major difference from previous BdG calculations is that, instead of an impurity potential [51, 52] to account for the charge disorder, we have fixed the initial local charge densities throughout the calculations in order to take into account the results of the CH approach and also in agreement with the data on stripe formation [4, 30]. This novel procedure is necessary to study the formation of the superconducting regions on the local density patterns which results from the phase separation process as shown, for instance, in figures 1 and 2. In the next section, we perform the superconducting calculations with d-wave symmetry for clusters with disordered local charge.

4. Results

We perform the BdG calculations on clusters of uniform density ranging from zero to $p_{\rm m} = 0.3$ with parameters which make the values of $T_{\rm c}(p_{\rm m})$ vanish near these limits, as listed below equation (2). Then we perform calculations with inhomogeneous clusters and concentrate on the stripe geometry which occurs in LSCO [4]. We connect the stripe phase with the above CH results through a scheme displayed in figure 4, where the value of X is related to the degree of the phase separation. Due to the large values of $T_{\rm ps}(p_{\rm m})$ at the strong underdoped regime, the level of phase separation is maximum at low temperatures, and $X = 0$ for doping values of $p_{\rm m} \leqslant 0.05$. For $0.12 \leqslant p_{\rm m} \leqslant 0.19$ the values of X may build up to 0.05. Notice that when $X = 0$ the charge distribution is a bimodal with the system divided into two distinct regions; insulator with $p(i) \approx 0.0$ and metallic with $p(i) \approx 2p_{\rm m}$.

In this case the metallic regions are in the limit of percolation [55], but for $X = 0.04$ or bigger, despite the insulator regions present, the metallic character dominates over the entire system. This scheme is an approximate way to deal with the phase separation which leads to the stripe charge configuration of real systems.

Thus, the goal is to study the *local* pairing amplitude at a site $\mathbf{x_i}$ or simply 'i' as a function of temperature $\Delta(i, T)$ on clusters with charge stripes. Following the values of $\Delta(i, T)$ it is

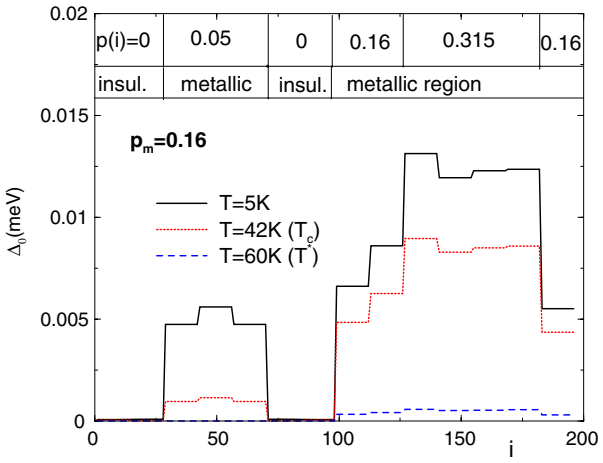

Figure 5. The temperature evolution of the local pairing amplitude $\Delta(i, T)$ (in units of eV) for systems with stripe disorder and average doping level of $p_m = 0.16$ with $T^* \approx 60$ K and $T_c \approx 42$ K. i here represents the sites of a $14 \times 14 = 196$ cluster.

possible to estimate $T_c(i)$ and to draw many interesting conclusions for the phase diagram. To explain our approach for an LSCO system with density inhomogeneity in stripe form, we will analyse the results for a cluster with $p_m = 0.16$ in a 14×14 cluster as shown in figure 5. At high temperatures but below $T_{ps}(p_m = 0.16) \approx 250$ K (this estimate is from figure 11 of [3]), the system is a disordered metal going through a continuous phase separation as the temperature is decreased. Below this temperature, say for $T \leqslant 200$ K, due to the continuous phase separation, a (LSCO) compound may be composed of six stripes with local charge density $p(i)$ given by 0.0–0.05–0.0–0.16–(0.32–0.05)–0.16. The low density regions are pictured on the left and the high density are on the right of the cluster (see figure 5) and one follows the other by periodic boundary conditions. These two markedly different regions provided an explanation for the dual behaviour detected by several ARPES measurements [11–14]. At high temperatures there are no superconducting regions in the sample, but at $T^* \gtrapprox 60$ K, as we can see in figure 5, some local superconducting amplitudes arise, forming superconducting islands in the most dense or metallic region. Thus this temperature ($T^* \approx 60$ K) is the onset of pair formation and we take it as the beginning of the pseudogap phase. Notice however that, at this ($T^* \approx 60$ K) temperature, these superconducting regions are weakly isolated from one another in the disordered metallic matrix [46–48] because the amplitudes of pairing (Δ) are very small, and non-vanishing only in the core of the metallic region as seen in figure 5. This figure also shows that upon cooling down the superconducting regions become more robust as the $\Delta(i, T)$ increases and new ones are built up where there are hole fluctuations (at X in figure 4) in the lightly doped regions. The induced pairing amplitude in the low density regions (at X) is possibly the origin of the superconducting phase through the percolation of the local superconducting islands with their phase locked, which favour the Josephson coupling. One can see in figure 5 that around 42 K the pairing amplitudes develop also at $X = p(i) = 0.05$, but for the $p_m = 0.06$ sample they develop even at $X = p(i) = 0.01$ (see figure 6) and thus the superconducting regions cover more than 50% of the CuO_2 plane. Consequently they percolate [55], and the whole system is able to hold a current without dissipation, that is, $T_c(p_m = 0.16) \approx 42$ K is the superconducting critical temperature for this compound.

Notice that the assumption that the order parameter has a rigid phase, as in a BCS superconductor, also has experimental support [56], although it is against the phase disordered

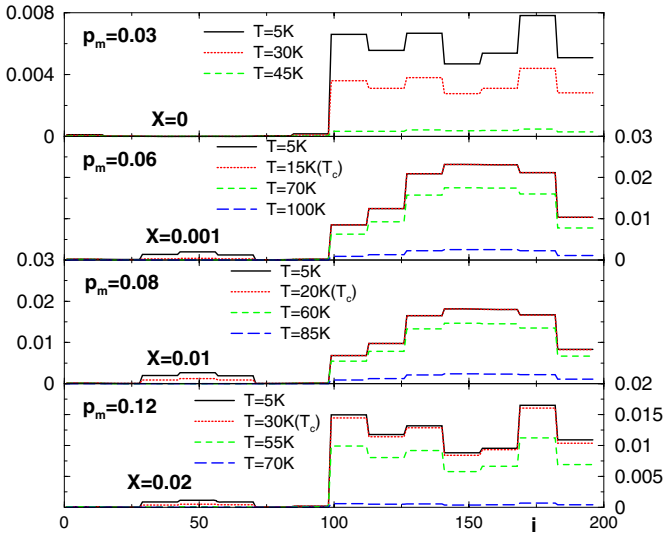

Figure 6. The temperature evolution of the local pairing amplitude $\Delta(i, T)$ (in units of eV) for systems with stripe charges with average doping level ranging from $p_m = 0.03$ to 0.12. The onset temperature (T_c) of percolation is shown in every panel.

scenario which lately has gained increased theoretical interest [7, 57]. It also makes possible the superconducting phase to be achieved by the Josephson coupling among the many local superconducting clusters.

We now apply this analysis to a series of compounds in order to show how the main features of the whole LSCO phase diagram can be derived. Our results are shown in figure 6 for mostly underdoped samples and in figure 7 for larger average doping values. For very lightly doped compounds like $p_m = 0.03$, due to the high values of $T_{ps}(p_m)$, there are stripes of only $p(i) = 0.0$ and $p(i) = 0.06$ separated by a small boundary with $p(i) = 0.03$. We considered a region metallic if it has a density of $p(i) \geqslant 0.04$–0.05; since the doped regions with $p(i) = 0.06$ occupy less than half the system, which is lower than the two dimensional percolation limit of 50–60% [55], this compound is not a metal, although it has a metallic behaviour at high temperatures [58]. Such behaviour can be explained as due to the holes which can tunnel over the dense $p(i) = 0.06$ stripe regions. This tunnelling can also be the origin of the zero temperature pseudo-gap (ZTPG) detected by STM [18–20]. For these underdoped compounds, the pairing amplitude develops strictly in the metallic or heavily doped regions (see the top panel of figure 7), and the superconducting islands occupy less than 50% of the available area, which is below the percolation limit.

For a compound with $p_m = 0.06$, T_{ps} is still very high; the density profile is characterized by a very small charge fluctuations around a bimodal distribution given by $X = 0.001$. The stripe regions have densities given by $p(i) = 0.0$–0.001–0.0–0.06–0.119–0.06. This system can be considered at the metallic limit, which is 50% of the sites with $p(i) \geqslant 0.04$. We see that the onset of superconducting islands is at $T^* = 100$ K and the percolation threshold occurs near $T_c = 15$ K, specially due to the already mentioned unexpected pairing amplitudes induced at the low density sites with $p(i) = 0.001$ (see figure 6). Thus for temperatures between $T = 15$ and 100 K the system is a poor metal with insulator, metallic and superconducting regions. The presence of these superconducting islands in many compounds is verified by several different experiments. Perhaps the most clear demonstration of these static superconducting

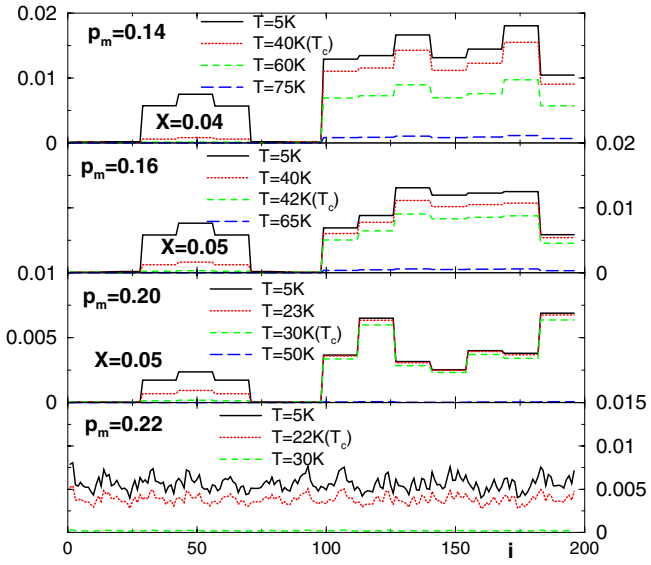

Figure 7. The temperature evolution of the local pairing amplitude $\Delta(i, T)$ (in units of eV) for systems with stripe disorder with average doping level ranging from $p_m = 0.14$ to 0.22. Notice that the $p_m = 0.22$ compound does not undergo a phase separation transition and its local density fluctuates around $p_m = 0.22$.

regions is through the tunnelling data [22, 28, 29], which have seen a (superconducting) gap well above T_c. More recently, measurements of the Nernst effect [59] also demonstrated the presence of the local superconducting regions above $T_c(p_m)$ although it was interpreted as due to superconducting fluctuations instead of the static cluster considered here. For compounds with an average doping larger than $p_m = 0.06$, we notice that the onset of superconductivity T^* decreases almost steadily, while the onset of percolation T_c goes through a maximum at the optimum doping $p_m = 0.16$. The reason for this behaviour in our calculation is the deviations from the bimodal distribution (given by the increase of the phase separation parameter X as in figure 4).

In the figure 7 we can see that the phase separation process and the local superconducting calculations follow a similar pattern up to $p_m = 0.20$. Following current trends [3, 42, 49], we assume that the phase separation ends at $p_m \approx 0.20$ and, for heavier doped compounds, the charge disorder is very weak like a small fluctuation around the average value p_m, similar to the charge distribution shown in figure 3(a). This is the same kind of charge fluctuation which occurs above the phase separation transition temperature T_{ps}. Consequently, the compound with $p_m = 0.22$ differs greatly from the other compounds shown in figure 7, and it has only local densities $p(i) \approx 0.22$, which is in the metallic range. The local pairing amplitudes $\Delta(i, T)$ are built in the whole system at $T = 30$ K and not in islands or droplets. If we adhere to the assumption that T^* is the onset of superconducting correlations, we see that, for these $p_m \geqslant 0.20$ overdoped samples, T^* merges into T_c. The other important consequence is that the normal phase is much more homogeneous, without insulating and superconducting regions, than the $p_m \leqslant 0.20$ compounds. This is seen experimentally through the Fermi liquid behaviour of many measurements carried in the heavily overdoped regime together with the absence of a pseudogap [2, 7].

In figure 8 we used the calculated local $\Delta(i, T)$ on each compound to derive the LSCO phase diagram, to wit, the onset of superconducting temperature $T^*(p_m)$ (squares) and the

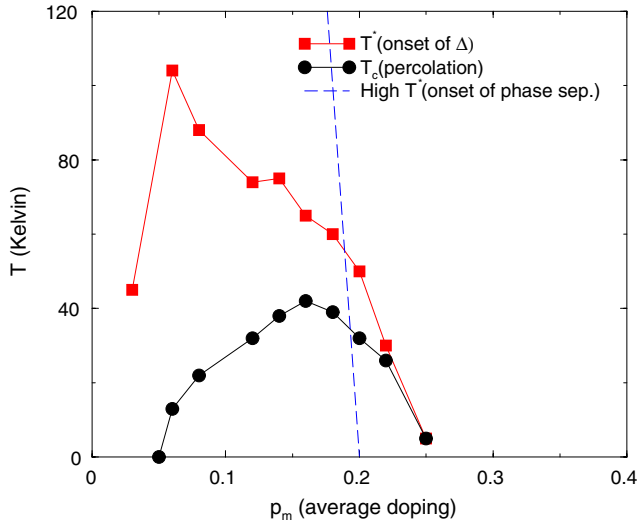

Figure 8. The onset of superconducting island temperature $T^*(p_m)$ and the possible percolation temperature $T_c(p_m)$ taken from figures 7 and 6. The phase separation (dashed) line or upper pseudogap is also shown [3, 49].

percolation temperature $T_c(p_m)$ (circles) as a function of p_m, as derived from figures 7 and 6. The values of $T^*(p_m)$ are in good agreement with the measurements attributed to the lower pseudogap line, which is usually related to the onset of a superconducting property [2, 3, 42], for instance the tunnelling results [22, 29] and the Nernst effect [59]. The values of $T_c(p_m)$ are also in good quantitative agreement with the experimental superconducting phase boundary [2, 3, 59].

We have also taken the larger $\Delta(i, T = 0)$ for each compound from the calculations similar to those shown in figures 6 and 7 and plotted in figure 9. These maximum pairing amplitudes for each p_m at low temperature ($\Delta_0(p_m)$) are in reasonable agreement with the ARPES zero temperature leading edge shift or the maximum magnitude of the superconducting gap [14]. The pairing amplitude and the superconducting gap are equal for a homogeneous system but, as shown by Ghosal *et al* [52], their difference increases with the disorder. In our two component system the maximum pairing amplitude develops inside the metallic region where the sites have a fairly homogeneous density, that is, $p(i) \approx 2p_m$. Since the opening of this maximum $\Delta(i, T = 0)$ is associated with the onset of superconductivity or pseudogap temperature $T^*(p_m)$, it is reasonable to take it equal to the maximum zero temperature superconducting gap $\Delta_0(p_m)$. In this figure 9, to study also the effect of the disorder in our calculations, we have shown the values of $\Delta_0(p_m)$ for homogeneous compounds (which is in this case equal the superconducting gap). We see that the disorder increases the average zero temperature gap dramatically at low doping and in a weaker way in the far overdoped regions. The discrepancies around optimally doped samples between the experimental leading edge values and our calculations are likely to be due to our approximate stripe configurations on small clusters.

It is important to notice that this phase separation scheme is able to capture the very curious dual behaviour of the electronic structure in LSCO systems [12]. At the lightly doped regime, due to the high values of the phase separation energy barrier $E_g(T, p_m)$, the charges move preferably along the high density stripes, and the Cooper pairs are formed along them, as

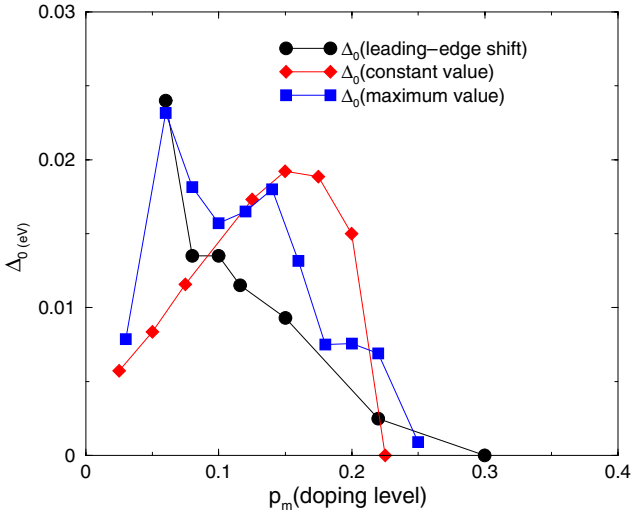

Figure 9. The maximum pairing amplitude $\Delta_0(p_m)$ as a function of the doping level. The diamond points are for a cluster with uniform density. The squares are for an inhomogeneous cluster following to the CH results. The circles are the experimental leading edge gap from [14].

demonstrated in figures 6 and 7 by the calculated $\Delta(i, T = 0\ \mathrm{K})$. Consequently, with a k-space probe, the superconducting gaps for lightly doped samples are measured mainly in the $(\pi, 0)$ and $(0, \pi)$ antinodal regions and the spectral weight segments are entirely near these antinodal regions. This behaviour is expected for 1D stripes [12] and the measured values of the zero temperature leading edge as a function of p_m can be reasonably reproduced by the values of $\Delta_0(p_m)$, as shown in figure 9.

Since by assumption $E_g(T, p_m)$ is closely related to the high pseudogap and, therefore, decreases rapidly with p_m, it is easier for the holes in compounds near optimally doped than underdoped ones to tunnel over among the high and low doping stripes, yielding a 2D character of these systems. Thus as p_m increases, the samples tend to change continuously from 1D to a 2D metallic behaviour and this is detected by the increase of the spectral weight near the Fermi surface along the [1,1] nodal direction [12]. Another evidence of the charge tunnelling between different stripes is the presence of the incoherent ZTPG measured on the surface of Bi2212 compounds [18, 19], which should scale with the energy barrier $E_g(p_m, T)$. The ZTPG are more frequently than the superconducting gap in the underdoped region and disappear near $p_m = 0.19$ [18–20]. Evidence of these two types of gaps in HTSC compounds came also from tunnelling experiments carried out with different resistances [28, 29].

5. Conclusions

We have worked out a complete scenario for HTSC and provided an interpretation for the upper and lower pseudogap lines and also for the superconducting phase. Taking the upper pseudogap as the phase separation temperature, we have calculated the order parameter local pairing amplitudes $\Delta(i, T)$, which, as in BCS, are assumed to have their phase locked, and the superconducting phase is reached probably by percolation or Josephson coupling at $T_c(p_m)$. In this way, we derived the phase diagram from the onset of $\Delta(i, T)$, that is $T^*(p_m)$ and $T_c(p_m)$ for the LSCO family. Although the process of phase separation varies continuously with the temperature and depends on the sample preparation, for simplicity we use in our calculations

only the low temperature static configuration. Despite this simplification, the method is quite general, and to demonstrate it, we reproduced results in good agreement with the LSCO series.

The many values of $\Delta(i, T)$ at different locations of a single compound, assumed to be proportional to the local superconducting gap, agree with several recent STM data. The calculations with the CH stripe configuration have also provided a novel interpretation to important aspects involving the electronic structure of this type of disorder: the inhomogeneous electronic dual nature of underdoped LSCO cuprates measured by the straight (1D) segments near the anti-nodal regions and the spectral weight near the nodal regions where the Fermi surface develops. The presence of the ZTPG peaks in several Bi2212 compounds, as measured by high resolution STM data, may be due to the energy barrier between the low and high density regions ($E_g(T, p_m)$) in a given sample, and therefore, in this view, it is connected to the phase separation and not to the superconductivity. Our results indicate that the normal phase of cuprates is a disordered metal (for $p_m \leqslant 0.2$) composed by the coexistence of insulator and metallic regions below the phase separation temperature T_{ps}. These regions are composed of non-constant hole density droplets or islands with a variety of local $T_c(p(i))$ at low temperatures. This inhomogeneity is the source of scattering between these non-uniform regions, Andreev reflection, etc, which is the cause of many non-conventional transport properties [2, 7]. The study of these normal phase properties will be a matter of future publication.

Thus, in short, with the combination of the CH phase separation model with the BdG superconducting theory, we have shown that the phase diagram and some non-conventional properties of HTSCs receive a coherent interpretation based on a temperature dependent phase separation.

Acknowledgments

This work has been partially supported by CAPES, CNPq and CNPq-Faperj Pronex E-26/171.168/2003.

References

[1] See discussion in 2006 *Nature Phys.* **2** (3)
[2] Timusk T and Statt B 1999 *Rep. Prog. Phys.* **62** 61
[3] Tallon J L and Loram J W 2001 *Physica* C **349** 53
[4] Tranquada J M, Sternlieb B J, Axe J D, Nakamura Y and Uchida S 1995 *Nature* **375** 561
[5] Pan S H *et al* 2001 *Nature* **413** 282–5 (*Preprint* cond-mat/0107347)
[6] Hanaguri T, Lupien C, Kohsaka Y, Lee D-H, Azuma M, Takano M, Takagi H and Davis J C 2004 *Nature* **430** 1001
[7] Lee P A, Nagaosa N and Wen X-G 2006 *Rev. Mod. Phys.* **78** 17
[8] Bobroff J, Alloul H, Ouazi S, Mendels P, Mahajan A, Blanchard N, Collin G, Guillen V and Marucco J-F 2002 *Phys. Rev. Lett.* **89** 157002
[9] Loram J W, Tallon J L and Liang W Y 2004 *Phys. Rev.* B **69** 060502
[10] de Mello E V L and Caixeiro E S 2004 *Phys. Rev.* B **70** 224517
[11] Damascelli A, Hussain Z and Shen Z-X 2003 *Rev. Mod. Phys.* **75** 473
[12] Zhou X J, Yoshida T, Kellar S A, Bogdanov P V, Lu E D, Lanzara A, Nakamura M, Noda T, Kakeshita T, Eisaki H, Uchida S, Fujimori A, Hussain Z and Shen Z-X 2001 *Phys. Rev. Lett.* **86** 5578
[13] Zhou X J, Yoshida T, Lee D-H, Yang W L, Brouet V, Zhou F, Ti W X, Xiong J W, Zhao Z X, Sasagawa T, Kakeshita T, Eisaki H, Uchida S, Fujimori A, Hussain Z and Shen Z-X 2004 *Phys. Rev. Lett.* **92** 187001
[14] Ino A, Kim C, Nakamura M, Yoshida T, Mizokawa T, Fujimori A, Shen Z-X, Kakeshita T, Eisaki H and Uchida S 2002 *Phys. Rev.* B **65** 094504
[15] Howald C, Fournier P and Kapitulnik A 2001 *Phys. Rev.* B **64** 100504
[16] Lang K M, Madhavan V, Hoffman J E, Hudson E W, Eisaki H, Uchida S and Davis J C 2002 *Nature* **415** 412

[17] Hoffman J E, McElroy K, Lee D-H, Lang K M, Eisaki H, Uchida S and Davis J C 2002 *Science* **297** 1148–51
[18] McElroy K, Simmonds R W, Hoffman J E, Lee D-H, Orenstein J, Eisaki H, Uchida S and Davis J C 2003 *Nature* **422** 520
[19] Fang A C, Capriotti L, Scalapino D J, Kivelson S A, Kaneko N, Greven M and Kapitulnik A 2006 *Phys. Rev. Lett.* **96** 017007
[20] McElroy K, Lee D-H, Hoffman J E, Lang K M, Lee J, Hudson E W, Eisaki H, Uchida S and Davis J C 2005 *Phys. Rev. Lett.* **94** 197005
[21] Vershinin M, Misra S, Ono S, Abe Y, Ando Y and Yazdani A 2004 *Science* **303** 1995
[22] Renner Ch, Revaz B, Genoud J Y, Kadowaki K and Fischer O 1998 *Phys. Rev. Lett.* **80** 149
[23] Miyakawa N, Guptasarma P, Zasadzinski J F, Hinks D G and Gray K E 1998 *Phys. Rev. Lett.* **80** 157
[24] Suzuki M and Watanabe T 2000 *Phys. Rev. Lett.* **85** 4787
[25] Deutscher G 1999 *Nature* **397** 410
[26] Krasnov V M, Kovalev A E, Yurgens A and Winkler D 2001 *Phys. Rev. Lett.* **86** 2657
[27] Yurgens A, Winkler D, Claeson T, Ono S and Ando Y 2003 *Phys. Rev. Lett.* **90** 147005
[28] Mourachkine A 2000 *Physica* **341–348** 917
[29] Mourachkine A 2005 *Mod. Phys. Lett.* B **19** 743 (*Preprint* cond-mat/0506732) (Review article)
[30] Bianconi A, Saini N L, Lanzara A, Missori M, Rossetti T, Oyanagi H, Yamaguchi H, Oda K and Ito T 1996 *Phys. Rev. Lett.* **76** 3412
[31] Bozin E S, Kwei G H, Takagi H and Billinge S J L 2000 *Phys. Rev. Lett.* **84** 5856
[32] Curro N J, Hammel P C, Suh B J, Hcker M, Bchner B, Ammerahl U and Revcolevschi A 2000 *Phys. Rev. Lett.* **85** 642
[33] Singer P M, Hunt A W and Imai T 2002 *Phys. Rev. Lett.* **88** 047602
[34] Haase J, Sushkov O P, Horsch P and Williams G V M 2004 *Phys. Rev.* B **69** 094504
[35] Grafe H J, Curro N J, Hcker M and Bchner B 2006 *Phys. Rev. Lett.* **96** 017002
[36] Zaanen J and Gunnarson O 1989 *Phys. Rev.* B **40** 7391
[37] Kato M, Machida K, Nakanishi H and Fujita M 1990 *J. Phys. Soc. Japan* **59** 1047
[38] Grenier J C, Lagueyte N, Wattiaux A, Doumerc J P, Dordor P, Etourneau J, Puchard M, Goodenough J B and Zhou J S 1992 *Physica* C **202** 209
[39] Jorgensen J D, Dabrowski B, Pei S, Hinks D G, Soderholm L, Morosin B, Schirber J E, Venturini E L and Ginley D S 1988 *Phys. Rev.* B **38** 11337
[40] Truccato M, Lamberti C, Prestipino C and Agostino A 2005 *Appl. Phys. Lett.* **86** 213116 (*Preprint* cond-mat/506198)
[41] Kristoffel N and Rubin P 2004 *Physica* C **402** 257
[42] Markiewicz R S 2002 *Phys. Rev. Lett.* **89** 229703
[43] Cahn J W and Hilliard J E 1958 *J. Chem. Phys.* **28** 258
[44] de Mello E V L and Silveira Filho O T 2005 *Physica* A **347** 429
[45] de Mello E V L and Caixeiro E S 2006 *J. Phys. Chem. Solids* **67** 165
[46] Ovchinnikov Yu N, Wolf S A and Kresin V Z 2001 *Phys. Rev.* B **63** 064524
Ovchinnikov Yu N, Wolf S A and Kresin V Z 2000 *Physica* C **341–348** 103
[47] de Mello E V L, Caixeiro E S and González J L 2003 *Phys. Rev.* B **67** 024502
[48] González J L and de Mello E V L 2004 *Phys. Rev.* B **69** 134510
[49] Naqib S H, Cooper J R, Tallon J L, Islam R S and Chakalov R A 2005 *Phys. Rev.* B **71** 054502
[50] Franz M, Kallin C, Berlinsky A J and Salkola M I 1997 *Phys. Rev.* B **56** 7882
[51] Ghosal A, Randeria M and Trivedi N 2000 *Phys. Rev.* B **63** R020505
[52] Ghosal A, Randeria M and Trivedi N 2001 *Phys. Rev.* B **65** 014501
[53] Nunner T S, Andersen B M, Melikyan A and Hirshfeld P J 2005 *Phys. Rev. Lett.* **95** 177003
[54] Schabel M C, Park C-H, Matsuura A, Shen Z-X, Bonn D A, Liang X and Hardy W N 1998 *Phys. Rev.* B **57** 6090
[55] Stauffer D and Aharony A 1994 *Introduction to Percolation Theory* 2nd edn (Bristol: Taylor and Francis)
[56] Bergeal N, Leuseur J, Aprili M, Faini F, Contour J P and Leridon B 2006 *Preprint* cond-mat/0601265
[57] Emery V J and Kivelson S A 1995 *Nature* **374** 434
[58] Yoshida T, Zhou X J, Sasagawa T, Yang W L, Bogdanov P V, Lanzara A, Hussain Z, Mizokawa T, Fujimori A, Eisaki H, Shen Z-X, Kakeshita T and Uchida S 2003 *Phys. Rev. Lett.* **91** 027001
[59] Wang Y, Li L and Ong N P 2006 *Phys. Rev.* B **73** 024510